Cross-linkable Fullerene Derivatives for Solution-processed n–i-p Perovskite Solar Cells

Konrad Wojciechowski[1,†], Ivan Ramirez[1,†], Therese Gorisse[2], Olivier Dautel[3], Raghunath Dasari[4], Nobuya Sakai[1], Josue Martinez Hardigree[1], Seulki Song[5], Seth Marder[4], Moritz Riede[1], Guillaume Wantz[2], Henry J. Snaith[1,*]

† These authors contributed equally, * henry.snaith@physics.ox.ac.uk

Addresses

1. *Clarendon Laboratory, University of Oxford, Parks Road, OX1 3PU, United Kingdom*. 2. *IMS laboratory. Bordeaux Institute of Technology (IPB), University of Bordeaux, CNRS UMR 5218, ENSCBP, 16 Pey Berland, 33607 Pessac Cedex, France*. 3. *Hétérochimie Moléculaire et Macromoléculaire UMR CNRS 5076, Ecole Nationale Supérieure de Chimie de Montpellier, 8 rue de l'Ecole Normale 34296 Montpellier Cedex 05, France.* 4. *School of Chemistry and Biochemistry and Center for Organic Photonics and Electronics, Georgia Institute of Technology, Atlanta, GA 30332, USA*, 5. *Department of Chemical Engineering, Pohang University of Science and Technology (POSTECH), San 31, Nam-gu, Pohang, Kyungbuk 790-784, Korea*

Abstract

Hybrid perovskites form an extremely attractive class of materials for large scale, low-cost photovoltaic applications. Fullerene-based charge extraction layers have emerged as a viable n-type charge collection layer and in “inverted” p-i-n device architectures the solar cells are approaching efficiencies of 20%. However, the regular n-i-p devices employing fullerenes still lag behind in performance. Here, we show that partial solubility of fullerene derivatives in the aprotic solvents used for the perovskites, make it challenging to retain integral films in multilayer solution processing. To overcome this issue we introduce cross-linkable fullerene derivatives as charge collection layers in n-i-p planar junction perovskite solar cells. The cross-linked

fullerene layers are insolubilized, and deliver improved performance in solar cells, enabled by a controllable film thickness.

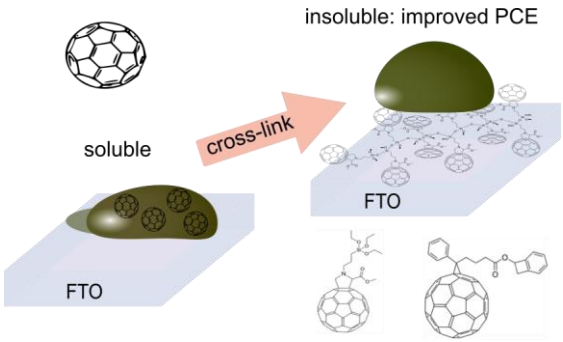

Metal halide perovskites constitute a very attractive class of materials for optoelectronic applications, such as solar cells, light emitting diodes, lasers and photodetectors.[1–8] Most notably, solid-state photovoltaic devices based on these materials have reached power conversion efficiencies (PCEs) of 22% after less than 4 years of academic research.[1,9,10,11] One of the central challenges in pushing the photovoltaic performance of perovskite cells closer to the thermodynamic limit is eliminating non-radiative recombination pathways.[12,13] These losses are understood to primarily occur due to trap-assisted recombination sites, most likely located at the interfaces between the charge selective contacts and the perovskite absorber layer.[14,15] In addition to trapping sites, which are present in all semiconductors, metal halide perovskites display mixed ionic and electronic conduction,[16] which has several implications on the device operation.[17,18] In the presence of surface charge recombination sites, ion migration to the charge selective interfaces can enhance or further impede photovoltaic performance.[19] This effect, which leads to device performance dependent upon the light exposure and electronic bias history, manifested as hysteresis in the current-density voltage (JV) curves, is now supported by considerable experimental evidence.[20–23] Recently it was demonstrated that this effect occurs only in the presence of interfacial traps or a fast surface recombination velocity.[24–26]

We have previously shown that the planar junction between the perovskite and the compact TiO_2, which is commonly used for electron collection in n-i-p planar heterojunction architectures (see device schematic in **Figure 1c**), is not always ideal for efficient charge extraction.[15,27] To circumvent this issue, we have demonstrated that appropriate interface engineering of the n-type contact can dramatically improve the device operation and reduce the "anomalous hysteresis" in the JV curves. Fullerene-based molecules appear to be better candidates for making good electronic contact with perovskite absorber layers, and do not appear to induce such a high density of defects responsible for charge recombination at this heterojunction.[14,15,27–30] Nevertheless, their solubility in organic solvents, such as *N*,*N*-dimethylformamide (DMF) and chlorobenzene, which are commonly used for processing the perovskite i- and the organic p-layers in the device stack, limits the versatility of processing routes and makes multi-layer device fabrication challenging: Partial dissolution of the n-type charge collection layer is expected to create shunting paths, which exuberate hysteresis.[27] For organic semiconductors, chemical modification, which can trigger bonding of the individual molecules or polymer units, is often applied to increase the material's mechanical and thermal stability[31], as well as its solvent resistance.

Here, we show that indeed, conventional C60 films suffer from non-uniformity and partial dissolution when employed as the n-type charge collection layer beneath a perovskite thin film in perovskite solar cells. To overcome this issue, we employ two approaches to generate insolublized fullerene films as robust n-type charge collection layers for use with solution-processed perovskite films. On one approach is based on incorporation of a fullerene into a hybrid sol-gel film and the other is based on incorporation of a ring opening reaction of a benzocyclobutene derivative of a fullerene. Both approaches yield films that are predominantly insoluble in the relevant solvents after the crosslinking reaction, which results in significantly reduced shunting paths and improved hole-blocking properties. This, combined with efficient

electron extraction from the perovskite layer, leads to enhanced steady-state power conversion efficiency.

When fabricating n-i-p perovskite solar cells, the n-type charge collection layer is first coated with the perovskite salts from an aprotic DMF solution, and then following curing and crystallisation of the perovskite film, it is coated with the organic p-type charge collection material from an organic solvent, typically chlorobenzene (CB) (**Figure 1a**). Since DMF and CB fully wash away the neat C_{60} layers[27], it is surprising these charge collection layers work at all in perovskite solar cells. However, when the DMF solution is loaded with ions, its ability to solvate the C_{60} film may change.

To determine whether C_{60} is washed away or remains after coating with the perovskite solution, we first coat the fullerene films with perovskite (MAI:$PbCl_2$ 3:1 ratio 40wt% in DMF), and then dissolve and remove the perovskite layer by dipping the films in γ-butyrolactone (GBL), which is a selective solvent for perovskite but not the C_{60} layer. We find that the C_{60} layer is still present on the FTO substrate with only around 50% reduced absorbance after this procedure (see **Figure 1b**). This confirms that some C_{60} remains after the perovskite film deposition. However, the reduced absorption is indicative of thinning of the C_{60} layer, which is unlikely to be uniform and homogeneous.

We note Seok and co-workers have employed GBL as the perovskite solvent, and managed to obtain uniform smooth films via the anti-solvent method, avoid dissolution of the underlying fullerene[30]. However, this approach offers limited flexibility in the processing of the perovskite.

For the “inverted” p-i-n perovskite solar cell architectures, the optimum thickness of the C60 layer has been found to be only 7 nm, with a relatively rapid drop off in solar cell performance for increasing or reducing this thickness by more than a few nm either side. Therefore, achieving such control over the film thickness, with such an apparent intolerance to thickness variation, is unlikely to be achievable, especially over larger areas, if the fullerene layer is being

partially washed away in an uncontrollable manner. Accordingly, the fullerene layer needs to be insoluble in DMF and also CB, the latter is important for the instances when pinholes exist in the perovskite films.

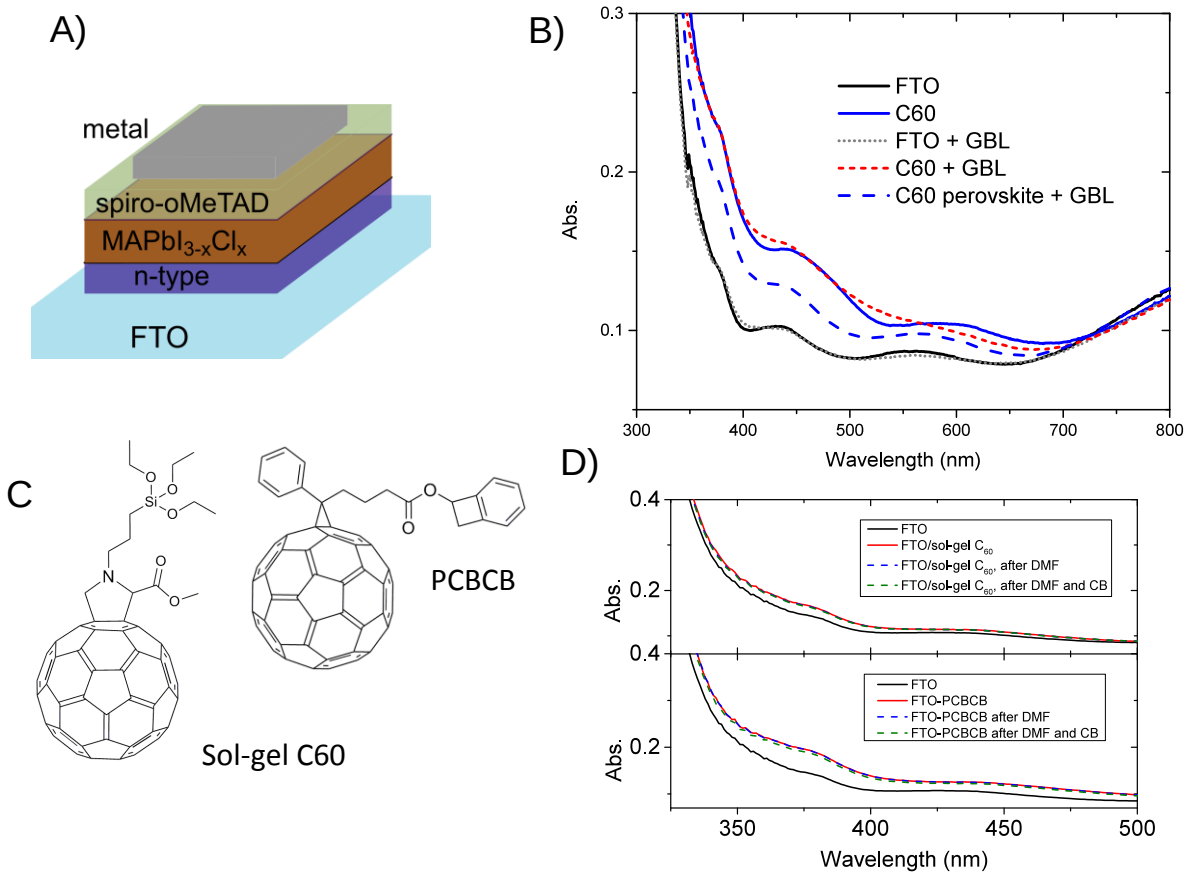

Figure 1. A) illustration of an n-i-p perovskite solar cell; B) UV-vis spectra of C60 films before (solid blue line) and after the deposition and removal (dashed blue line) of perovskite with γ-butyrolactone**.** The effect of this solvent on C60 is also measured (short dash red line). C) Chemical structures of the sol-gel C_{60} and PCBCB molecules. D) Effect of the neat solvents on cross-linked films. AFM topographical and phase images and the associated histograms before and after application of solvent can be found in **Figures S9 and S10.** We note that the shifts at long wavelengths in the UV-vis spectroscopy data are due to interference.

The first crosslinking approach we investigate here involves a fulleropyrrolidine derivative containing a triethoxysilane moiety (N-[3-(Triethoxysilyl)propyl]-2-carbomethoxy-3,4-fulleropyrrolidine), which we term sol-gel C_{60} (we show the chemical structure in **Figure 1c**). The molecule was developed by Bianco *et al*. for molecular recognition applications.[32] We deposited the sol-gel C_{60} films by spin-coating from solution in 1,2-dichlorobenzene, and induced crosslinking by exposure to trifluoroacetic acid (TFA) vapour. During the hydrolysis-condensation reactions the ethoxy groups of the sol-gel C_{60} are eliminated while Si-O-Si bonds are formed. We monitor the transformation in the sol-gel C_{60} FTIR spectrum, which we show in the Supporting Information (**Figure S6a**).

For our second insolublization approach, we employ a phenyl-C61-butyric acid methyl ester (PCBM) derivative with a benzocyclobutene group, phenyl-C61-butyric acid benzocyclobutene ester (PCBCB), the chemical structure of which we show in **Figure 1c**. The crosslinking occurs via thermal activation of the benzocyclobutene moiety and requires annealing at 200 °C for 10 minutes, as recently described by Deb *et al*.[33] In contrast to our investigations of the neat C_{60} layers, both UV-vis absorption and/or atomic force microscopy (AFM) on the sol-gel C_{60} films (6mg/ml) before and after application of neat DMF or CB show little change (**Figure 1d**). This indicates that the crosslinked fullerene films should enable much better optimisation of film thickness, and improved homogeneity of fullerene film thickness. We do note however, that height and phase histograms from the AFM images, which we present in **Figure S9 and S10**, suggest a few pinholes are present in the cross-linked fullerene layer after the application of neat DMF. This indicates that pinholes in the fullerene layers may become problematic, especially for extremely thin layers.

The electron mobility values of PCBCB, determined from space-charge limited current (SCLC) measurements, before and after crosslinking, have been reported by Deb *et al*.[33] After PCBCB polymerisation, the mobility substantially increases, exceeding the value of the reference

PCBM (see Table 1). We characterise the electron mobility in sol-gel C_{60} films by SCLC (Supplementary information, **Figure S12**), and summarise the mobility values in **Table 1**. As compared to PCBM, we observe a factor of 3 lower electron mobility for the sol-gel C_{60} film, after the crosslinking reaction. Hence, we expect the optimal layer thickness to be thinner for sol-gel C60 than for PCBCB, since we observe the highest mobility for the latter.

Table 1. Electron mobilities for the fullerene derivatives, determined from SCLC measurements (PCBCB, literature values)

Molecule		Mobility, μ_e ($cm^2V^{-1}s^{-1}$), SCLC
PCBM-BCB	before crosslinking	$1.3 \times 10^{-4} \pm 0.3 \times 10^{-4}$ from Ref. 33
	after crosslinking	$5.9 \times 10^{-3} \pm 1.8 \times 10^{-3}$ from Ref. 33
sol-gel C_{60}	before crosslinking	$9.4 \times 10^{-4} \pm 1.5 \times 10^{-4}$
	after crosslinking	$3.8 \times 10^{-4} \pm 0.5 \times 10^{-4}$
PCBM reference		$9.1 \pm 1.0 \times 10^{-4}$ from Ref. 33 $1.05 \times 10^{-3} \pm 0.2 \times 10^{-3}$

We present scanning electron microscopy (SEM) images of the spin-coated and cross-linked films, without the application of solvent, in **Figure S8**. Substrate cleaning plays a crucial role in achieving uniform and smooth films. We employ piranha etching to oxidize organic residues present on the FTO surface, which results in clean surfaces with improved wetting properties and gives films with very few visible fullerene aggregates. We produce uniform layers of the sol-gel C_{60} from solutions of concentration as low as 2 mg/ml, which yield a film thickness below 10 nm (as estimated from surface profileometry from solutions cast from 10mg/ml solutions, which yield films of 50nm thickness). We note that fullerene derivatives tend to aggregate over time in solution, but at the concentration range we use here (2-6 mg/ml) the solutions are stable for a period of a few weeks.

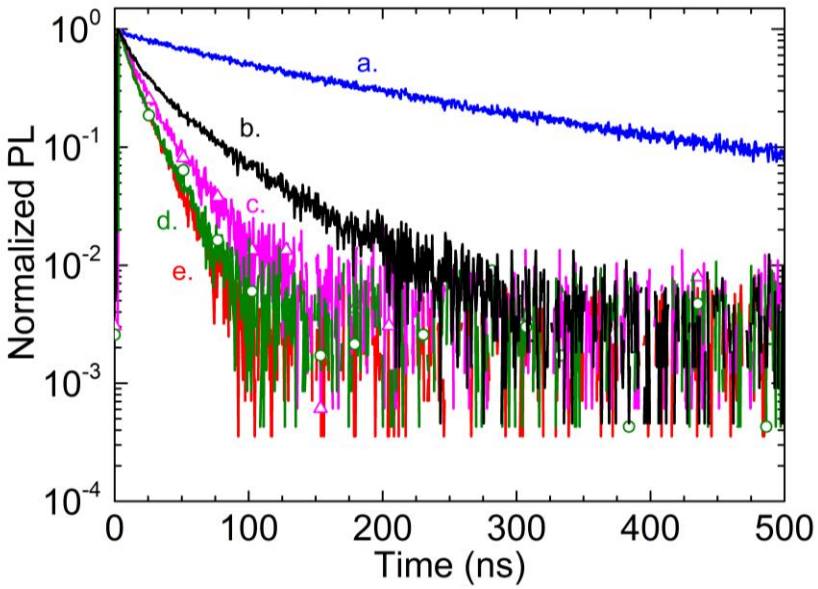

Figure 2, normalised photoluminescence decays (time correlated single photon counting) following pulsed excitation (507 nm, 1MHz, 0.03 µJ/cm^2/pulse) of the perovskite, both with and without the electron collection layer. a.: perovskite, b.: compact TiO2/perovskite c.: PCBCB/perovskite, d.: sol-gel C60/perovkite, e.: C60/perovskite.

In order to assess the efficacy of electron transfer from perovskite to the different fullerenes layers, we perform time-correlated single photon counting (TCSPC) measurements of $MAPbI_{3-x}Cl_x$ films processed on glass, and glass coated with different electron accepting layers (TiO_2, C_{60}, and both cross-linked fullerenes). We show the transient PL traces of all the samples in **Figure 2**, and the decay lifetimes we extract from the data in table 2. Similarly to previous reports,[34,35] we observe that the perovskite PL lifetimes are significantly shorter for the samples with a fullerene-based electron collection layer, as compared to those with a compact TiO_2 layer. The fast PL decay indicates rapid transfer of electrons from the perovskite into the fullerene layer, following photogeneration. We note that for cross-linked PCBCB, the PL quenching is slower than for cross-linked sol-gel C_{60} or neat C_{60}, which may be indicative of a poorer electronic coupling and slower charge extraction rate at the PCBCB-perovskite heterojunction.

Table 2. Lifetimes extracted from the photolumiscence decays in Figure 2, using bi-exponential decay fits $A_1 e^{-(t_1 - \Delta t)/t_1} + A_2 e^{-(t_2 - \Delta t)/t_1}$ where Δt is a correction for the time offset in the data. Fitting range was kept to 150ns for all fullerenes.

Sample	τ_1 /ns (A_1)	τ_2/ns (A_2)
Perovskite	51.8 (0.19)	189.8 (0.75)
TiO_2/Perovskite	12.8 (0.60)	53.3 (0.45)
Sol-gel C60/Perovskite	5.65 (0.38)	18.2 (0.62)
PCBCB/Perovskite	7.89 (0.42)	24.4 (0.58)
C60	3.60 (0.15)	15.2 (0.8)

Having established that both cross-linked fullerene films match the requirements for good electron-selective contacts, we fabricate planar heterojunction perovskite solar cells, with cross-linked fullerene layers as the electron selective contacts. We employ solution-processed C_{60} (not cross-linked) as a reference n-type charge collection layer. We show the scanning electron microscopy (SEM) images of perovskite films grown on the different n-type materials in **Figure S11**.

We show the current density-voltage curves (JV) and stabilised power output (SPO) of the most efficient devices employing each n-type contact in **Figures 3a-b** (voltage is swept from forward bias to short-circuit in the JV curves), and report the photovoltaic parameters extracted from the JV curves in **Table 2**. Both of the new fullerene derivatives delivered solar cells with JV measured power conversion efficiency (PCE) of nearly 18%. We observe that the SPO efficiency, measured at close to maximum power point, is a little lower, at 16.6% and 15.2% for the cells incorporating the sol-gel C_{60} and PCBCB, respectively. For the best reference device, employing solution-processed C_{60} compact layer, we measure a JV PCE of 14.7%, and 13.9% SPO. We present the statistics of the photovoltaic parameters derived from JV curves and SPO measurements in **Figure 3c-d** and **Table 3**. We observe that the devices employing

the cross-linked fullerenes exhibit a significant improvement in all photovoltaic parameters, as compared to the devices employing neat C_{60}. The most noticeable difference is the enhancement in V_{OC} and J_{SC}, which may be related to the reduced shunting paths and improved hole blocking properties, which result from the avoided dissolution of the fullerene layer.

As we have discussed above, in p-i-n inverted perovskite solar cells the optimum fullerene layer thickness is only 7nm. Therefore, since the cross-linked layers are not being dissolved we also expect optimum performance to occur with relatively thin fullerene layers. Consistently, we process the films for the optimum PV performance from a solution of only 2 mg/ml (spinning rate: 2000 rpm), which yields a sub 10 nm thickness, which we extrapolate from surface profileometry thickness measurements on thicker films cast from higher concentration solutions. The cross-linked PCBCB film exhibit significantly higher electron mobility,[33] and consistently we find that the optimal solution concentration for casting the layer is 5 mg/ml (spinning rate: 2000 rpm), resulting in a film thickness of ca. 15 nm (which we extrapolate from profileometry of thicker films). We note that for the devices employing sol-gel C_{60}, we measure higher SPO values and better PCE_{stab}/PCE_{JV} ratio than those employing PCBCB. This indicates more pronounced hysteresis in the latter, consistent with the slower charge extraction, as suggested by the TCSPC data, or more pin-holes being present inducing faster recombination at this junction.

Overall, we observe markedly increased SPOs and V_{OC} for cells employing cross-linked fullerenes as compared to the solution processed C_{60} reference. We have previously observed that hysteresis is extreme in cells entirely devoid of a charge selective contact.[17] Our results are consistent with there being more regions where the C_{60} films are entirely washed away during the processing of the perovskite layer, than is the case for the insolubilized fullerene derivatives we employ here. Our observed device improvements are therefore explainable if we consider that surface charge recombination is rapid at the heterojunction between FTO and the

perovskite, and this surface recombination is accelerated or inhibited by the accumulation of negative or positive ionic charge, respectively, at this interface.[24,36]

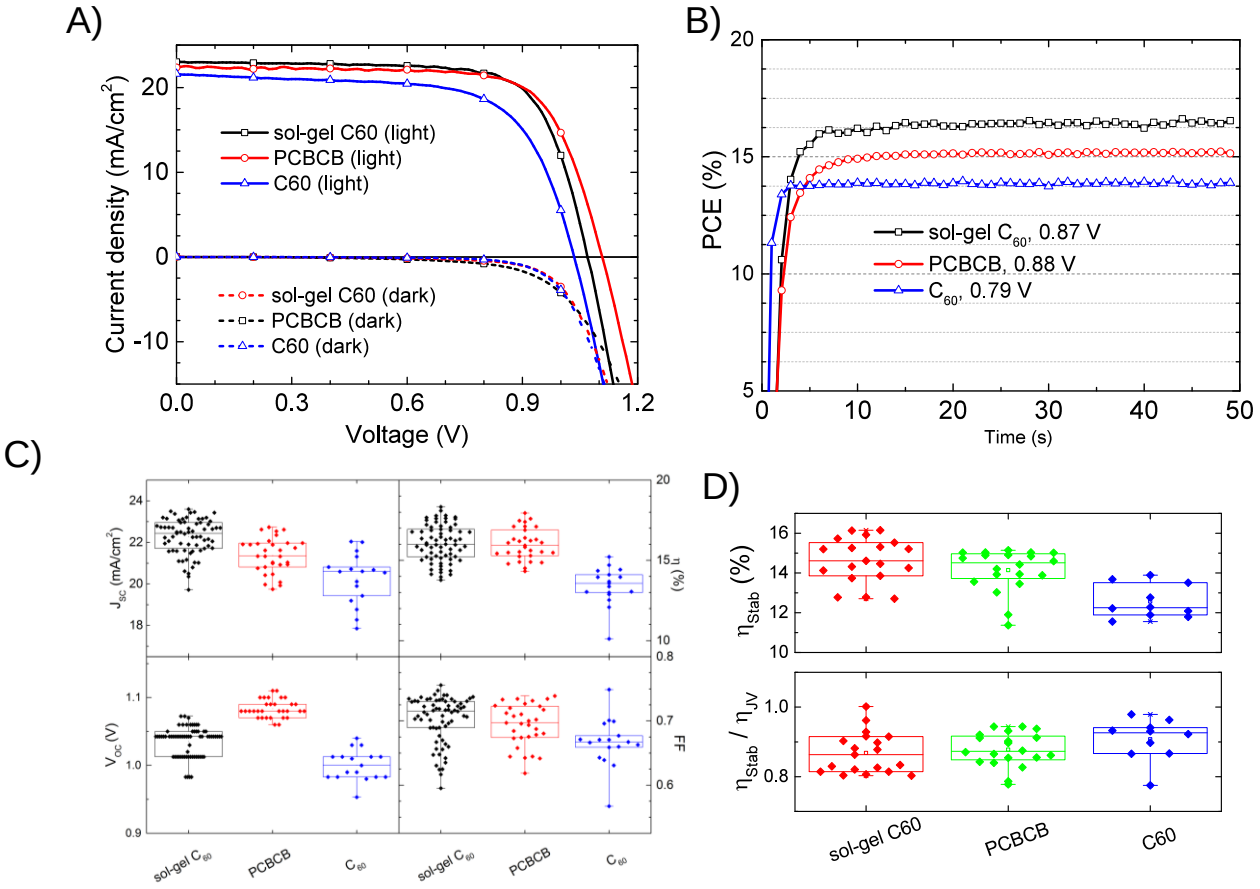

Figure 3. (a) Current density – voltage curves (FB-SC scan direction, 0.15 V/s) of the best devices employing different compact layers; **(b)** Stabilised power output of the same devices; statistics of **(c)** the JV curves (FB-SC scan direction, 0.15 V/s) and **(d)** SPO measurements for a larger set of devices. Each dot represents a single device.

Table 2. Photovoltaic Parameters Extracted from JV Curves presented in Figure 3a-b.

Compact layer	**FB-SC scan, 0.15 V/s**				**Stabilised**		
	J_{SC} (mA/cm^2)	V_{OC} (V)	FF	PCE (%)	J_{stab} (mA/cm^2)	PCE_{stab} (%)	PCE_{stab}/PCE_{JV}
sol-gel C_{60}	23.0	1.07	0.73	17.9	19.0	16.6	0.93
PCBCB	22.4	1.11	0.73	17.9	17.2	15.2	0.85

C_{60}	21.6	1.03	0.67	14.7	16.7	13.9	0.95

Table 3. Statistics of photovoltaic parameters (with standard deviation) presented in Figure 3c-d.

n-type layer	**FB-SC scan, 0.15 V/s**					**Stabilised**			
	No.	J_{SC} (mA/cm^2)	V_{OC} (V)	FF	PCE (%)	No.	J_{stab} (mA/cm^2)	PCE_{stab} (%)	PCE_{stab}/PCE_{JV}
sol-gel C_{60}	57	21.5±1.3	1.05± 0.03	0.67± 0.04	15.1±1.6	28	17.5±1.4	14.4±1.3	0.91±0.03
PCBCB	31	21.4±0.8	1.08± 0.01	0.69± 0.03	16.0±1.0	20	16.6±1.1	14.2±1.1	0.88±0.05
C_{60}	17	20.3±1.2	1.00± 0.02	0.67± 0.04	13.4±1.2	10	15.9±0.8	12.6±0.8	0.91±0.06

We have demonstrated that employing cross-linked fullerene layers is a viable means to greatly improve the n-type charge collection layer in solution processed perovskite solar cells. Now we have well operating insoluble organic n-type charge collection layers, we expect these materials, or this concept, to be of great importance for the upscaling of the solution processed perovskite PV technology, where thin films of high uniformity, high stability and well controlled thicknesses will be required to be compatible with rapid large area coating processes. In addition, there may be long term stability benefits due to cross-linking of these material, as has been observed with organic PV, due to inhibiting morphological changes and crystallisation of the fullerene layer, which could occur over extended periods of elevated temperatures.

Acknowledgements: K.W. gratefully acknowledges support from Oxford P.V. ltd and I.R. thanks EPSRC for providing a DTA studentship. This work was partially supported by EPSRC, the Air Force Office of Scientific Research (through grant FA9550-15-1-0115), the Department of the Navy, Office of Naval Research (Award Numbers N00014-14-1-0126 and N00014-14-1-0580) and by Framework Marie Skłodowska-Curie Action Career Integration Grant (630864).

Supporting information: the supporting information describes the experimental details relating to sample preparation and characterisation, material synthesis and purification. In addition SEM, AFM and SCLC data are presented.

Contributions: K.W. and I.R. designed/coordinated the project with input from all the authors. K.W., I.R. and T.G. optimised the thin films and assessed their solvent resilience and electronic quality. K. W. produced the devices, with help from N.S. O.D synthesised, purified and characterised the cross-linking of sol-gel C60, R. D. synthesised and purified PCBCB. JFMH performed AFM measurements. S.M, G.W, M.R. and HJS supervised the work.

References

(1) Lee, M. M.; Teuscher, J.; Miyasaka, T.; Murakami, T. N.; Henry, J. Efficient Hybrid Solar Cells Based on Meso-Superstructured Organometal Halide Perovskites. *Science* **2012**, *338*, 643–647.

(2) Tan, Z.-K.; Moghaddam, R. S.; Lai, M. L.; Docampo, P.; Higler, R.; Deschler, F.; Price, M.; Sadhanala, A.; Pazos, L. M.; Credgington, D.; et al. Bright Light-Emitting Diodes Based on Organometal Halide Perovskite. *Nat. Nanotechnol.* **2014**, *9*, 687–692.

(3) Cho, H.; Jeong, S.; Park, M.; Kim, Y.; Wolf, C.; Lee, C.; Heo, J. H.; Sadhanala, A.; Myoung, N.; Yoo, S.; et al. Overcoming the Electroluminescence Efficiency Limitations of Perovskite Light-Emitting Diodes. *Science* **2015**, *350*, 1222–1226.

(4) Zhu, H.; Fu, Y.; Meng, F.; Wu, X.; Gong, Z.; Ding, Q.; Gustafsson, M. V; Trinh, M. T.; Jin, S.; Zhu, X.-Y. Lead Halide Perovskite Nanowire Lasers with Low Lasing Thresholds and High Quality Factors. *Nat. Mater.* **2015**, *14*, 636–642.

(5) Deschler, F.; Price, M.; Pathak, S.; Klintberg, L. E.; Jarausch, D.; Higler, R.; Hu, S.; Leijtens, T.; Stranks, S. D.; Snaith, H. J.; et al. High Photoluminescence Efficiency and Optically Pumped Lasing in Solution-Processed Mixed Halide Perovskite Semiconductors. *J. Phys. Chem. Lett.* **2014**, *5*, 1421–1426.

(6) Fu, Y.; Zhu, H.; Schrader, A.; Liang, D.; Ding, Q.; Joshi, P.; Hwang, L.; Zhu, X.-Y.; Jin, S. Nanowire Lasers of Formamidinium Lead Halide Perovskites and Their Stabilized Alloys with Improved Stability. *Nano Lett.* **2016**, *16*, 1000–1008.

(7) Lin, Q.; Armin, A.; Burn, P. L.; Meredith, P. Filterless Narrowband Visible Photodetectors. *Nat. Photonics* **2015**, *9*, 687.

(8) Fang, Y.; Dong, Q.; Shao, Y.; Yuan, Y.; Huang, J. Highly Narrowband Perovskite Single-Crystal Photodetectors Enabled by Surface-Charge Recombination. *Nat. Photonics* **2015**, *9*, 679.

(9) Kim, H.-S.; Lee, C.-R.; Im, J.-H.; Lee, K.-B.; Moehl, T.; Marchioro, A.; Moon, S.-J.; Humphry-Baker, R.; Yum, J.-H.; Moser, J. E.; et al. Lead Iodide Perovskite Sensitized All-Solid-State Submicron Thin Film Mesoscopic Solar Cell with Efficiency Exceeding 9%. *Sci. Rep.* **2012**, *2*, 591.

(10) Kojima, A.; Teshima, K.; Shirai, Y.; Miyasaka, T. Organometal Halide Perovskites as Visible-Light Sensitizers for Photovoltaic Cells. *J. Am. Chem. Soc.* **2009**, *131*, 6050–6051.

(11) Green, M. A.; Emery, K.; Hishikawa, Y.; Warta, W.; Dunlop, E. D. Solar Cell Efficiency Tables (version 46). *Progress in Photovoltaics: Research and Applications*. July 19, 2015, pp 805–812.

(12) Yao, J.; Kirchartz, T.; Vezie, M. S.; Faist, M. a.; Gong, W.; He, Z.; Wu, H.; Troughton, J.; Watson, T.; Bryant, D.; et al. Quantifying Losses in Open-Circuit Voltage in Solution-Processable Solar Cells. *Phys. Rev. Appl.* **2015**, *4*, 014020.

(13) Miller, O. D.; Yablonovitch, E.; Kurtz, S. R. Strong Internal and External Luminescence as Solar Cells Approach the Shockley–Queisser Limit. *IEEE J. Photovoltaics* **2012**, *2*, 303–311.

(14) Shi, J.; Xu, X.; Li, D.; Meng, Q. Interfaces in Perovskite Solar Cells. *Small* **2015**, *11*, 2472–2486.

(15) Wojciechowski, K.; Stranks, S. D.; Abate, A.; Sadoughi, G.; Sadhanala, A.; Kopidakis, N.; Rumbles, G.; Li, C.; Friend, R. H.; Jen, A. K.; et al. Heterojunction Modification for Highly Efficient Organic-Inorganic Perovskite Solar Cells. *ACS Nano* **2014**, *8*, 12701–12709.

(16) Eames, C.; Frost, J. M.; Barnes, P. R. F.; O'Regan, B. C.; Walsh, A.; Islam, M. S. Ionic Transport in Hybrid Lead Iodide Perovskite Solar Cells. *Nat. Commun.* **2015**, *6*, 7497.

(17) Snaith, H. J.; Abate, A.; Ball, J. M.; Eperon, G. E.; Leijtens, T. C.; Noel, N. K.; Stranks, S. D.; Wang, J. T. W.; Wojciechowski, K.; Zhang, W. Anomalous Hysteresis in Perovskite Solar Cells. *J. Phys. Chem. Lett.* **2014**, *5*, 1511–1515.

(18) Unger, E. L.; Hoke, E. T.; Bailie, C. D.; Nguyen, W. H.; Bowring, A. R.; Heumüller, T.; Christoforo, M. G.; McGehee, M. D. Hysteresis and Transient Behavior in Current–voltage Measurements of Hybrid-Perovskite Absorber Solar Cells. *Energy Environ. Sci.* **2014**, *7*, 3690–3698.

(19) Tress, W.; Marinova, N.; Moehl, T.; Zakeeruddin, S. M.; Mohammad K., N.; Grätzel, M.; Nazeeruddin, M. K.; Grätzel, M. Understanding the Rate-Dependent J–V Hysteresis, Slow Time Component, and Aging in $CH_3NH_3PbI_3$ Perovskite Solar Cells: The Role of a Compensated Electric Field. *Energy Environ. Sci.* **2015**, *8*, 995–1004.

(20) Yuan, Y.; Chae, J.; Shao, Y.; Wang, Q.; Xiao, Z.; Centrone, A.; Huang, J. Photovoltaic Switching Mechanism in Lateral Structure Hybrid Perovskite Solar Cells. *Adv. Energy Mater.* **2015**, *5*, n/a-n/a.

(21) Leijtens, T.; Hoke, E. T.; Grancini, G.; Slotcavage, D. J.; Eperon, G. E.; Ball, J. M.; De Bastiani, M.; Bowring, A. R.; Martino, N.; Wojciechowski, K.; et al. Mapping Electric Field-Induced Switchable Poling and Structural Degradation in Hybrid Lead Halide Perovskite Thin Films. *Adv. Energy Mater.* **2015**, *5*, n/a-n/a.

(22) Li, C.; Tscheuschner, S.; Paulus, F.; Hopkinson, P. E.; Kießling, J. Iodine Migration and Its Effect on Hysteresis in Perovskite Solar Cells. *Adv. Mater.* **2016**, *28*, 2446–2454.

(23) Shao, Y.; Fang, Y.; Li, T.; Wang, Q.; Dong, Q.; Deng, Y.; Yuan, Y.; Wei, H.; Wang, M.; Gruverman, A.; et al. Grain Boundary Dominated Ion Migration in Polycrystalline Organic-Inorganic Halide Perovskite Films. *Energy Environ. Sci.* **2016**, 22–26.

(24) Reenen, S. Van; Kemerink, M.; Snaith, H. J. Modeling Anomalous Hysteresis in Perovskite Solar Cells. *J. Phys. Chem. Lett.* **2015**, *6*, 3808–3814.

(25) Xu, J.; Buin, A.; Ip, A. H.; Li, W.; Voznyy, O.; Comin, R.; Yuan, M.; Jeon, S.; Ning, Z.; McDowell, J. J.; et al. Perovskite–fullerene Hybrid Materials Suppress Hysteresis in Planar Diodes. *Nat. Commun.* **2015**, *6*, 7081.

(26) Shao, Y.; Xiao, Z.; Bi, C.; Yuan, Y.; Huang, J. Origin and Elimination of Photocurrent Hysteresis by Fullerene Passivation in $CH_3NH_3PbI_3$ Planar Heterojunction Solar Cells. *Nat. Commun.* **2014**, *5*, 5784.

(27) Wojciechowski, K.; Leijtens, T.; Siprova, S.; Schlueter, C.; Hörantner, M. T.; Wang, J. T. W.; Li, C. Z.; Jen, A. K. Y.; Lee, T. L.; Snaith, H. J. C_{60} as an Efficient N-Type Compact Layer in Perovskite Solar Cells. *J. Phys. Chem. Lett.* **2015**, *6* (12), 2399–2405.

(28) Tao, C.; Neutzner, S.; Colella, L.; Marras, S.; Ram, A.; Kandada, S.; Gandini, M.; Bastiani, M. De. 17.6% Stabilized Efficiency in Low-Temperature Processed Planar Perovskite Solar Cells. *Energy Environ. Sci.* **2015**, *8*, 2365–2370.

(29) Chueh, C.-C.; Li, C.-Z.; Jen, A. K.-Y. Recent Progress and Perspective in Solution-Processed Interfacial Materials for Efficient and Stable Polymer and Organometal Perovskite Solar Cells. *Energy Environ. Sci.* **2015**, *8*, 1160–1189.

(30) Ryu, S.; Seo, J.; Shin, S. S.; Kim, Y. C.; Jeon, N. J.; Noh, J. H.; Seok, S. Il. Fabrication of Metal-Oxide-Free $CH_3NH_3PbI_3$ Perovskite Solar Cells Processed at Low Temperature. *J. Mater. Chem. A* **2015**, *3*, 3271–3275.

(31) Derue, L.; Dautel, O.; Tournebize, A.; Drees, M.; Pan, H.; Berthumeyrie, S.; Pavageau, B.; Cloutet, E.; Chambon, S.; Hirsch, L.; et al. Thermal Stabilisation of Polymer-Fullerene Bulk Heterojunction Morphology for Efficient Photovoltaic Solar Cells. *Adv. Mater.* **2014**, *26*, 5831–5838.

(32) Bianco, A.; Gasparrini, F.; Maggini, M.; Misiti, D.; Polese, A.; Prato, M.; Scorrano, G.; Toniolo, C.; Villani, C. Molecular Recognition by a Silica-Bound Fullerene Derivative. *J. Am. Chem. Soc.* **1997**, *119*, 7550–7554.

(33) Deb, N.; Dasari, R. R.; Moudgil, K.; Hernandez, J. L.; Marder, S. R.; Sun, Y.; Karim, A.; Bucknall, D. G. Thermo-Cross-Linkable Fullerene for Long-Term Stability of Photovoltaic Devices. *J. Mater. Chem. A* **2015**, *3*, 21856–21863.

(34) Stranks, S. D.; Eperon, G. E.; Grancini, G.; Menelaou, C.; Alcocer, M. J. P.; Leijtens, T.; Herz, L. M.; Petrozza, A.; Snaith, H. J. Electron-Hole Diffusion Lengths Exceeding 1 Micrometer in an Organometal Trihalide Perovskite Absorber. *Science* **2013**, *342*, 341–344.

(35) Xing, G.; Mathews, N.; Sun, S.; Lim, S. S.; Lam, Y. M.; Grätzel, M.; Mhaisalkar, S.; Sum, T. C. Long-Range Balanced Electron- and Hole-Transport Lengths in Organic-Inorganic $CH_3NH_3PbI_3$. *Science* **2013**, *342*, 344–347.

(36) Richardson, G.; O'Kane, S.; Niemann, R. G.; Peltola, T.; Foster, J. M.; Cameron, P. J.; Walker, A. Can Slow-Moving Ions Explain Hysteresis in the Current-Voltage Curves of Perovskite Solar Cells? *Energy Environ. Sci.* **2016**, *9*, 1476–1485.